Walking droplets inside a chaotic stadium cavity

***Abstract*—Walking droplets gave the first macroscopic system discovered to exhibit wave-particle duality. A couple experimental tools are required for a proper control and measurement of such a system. The latter is generally ensured with costly equipment unreachable for most unfunded people. This paper proposes a complete low-cost and open-source experimental setup for walking droplets with a performance characterization. On the other hand, the stadium billiard, was introduced by Bunimovich as one of the first two-dimensional concave chaotic geometries. Drastic differences between classical and quantum particles behaviour were observed in such geometry. This papers gives the first observations of walking droplets inside a stadium billiard. It is observed that the walking droplet long-term evolution in a stadium billiard presents a clear scarring pattern, informing on the existence of preferred "probable positions".**

***Index Terms*—Walking droplet, Stadium, Experimental setup, Low-cost**

I. Introduction

Today, the most widely accepted interpretation of the quantum mechanics equations is the *Copenhagen* interpretation [1] which states that physical systems generally do not have definite properties prior to being measured, and that the measurement's possible results only obey a probability distribution that is predicted by quantum mechanics. It stands that this is the measurement which forces the collapsing of the wave function to only one of the possible values. However, many other currently non rejectable interpretations of quantum mechanics have been proposed [2]. These ones differ on such fundamental questions as whether quantum mechanics is deterministic or stochastic, which elements of quantum mechanics can be considered real, and what is the nature of measurement, among other matters. The *De Broglie* theory (distinguished from the de Broglie-Bohm association as discussed in [3]), on the contrary of the Copenhagen interpretation, is a deterministic theory that associates a real pilot-wave that is created by the particle itself and guides its motion inside the space. It considers that the particle has, at any time, a definite and real position. This particle's position is practically unknown, but can be statistically predicted by the *guiding equation* [4]. In the *De Broglie* theory, the wave function obeying the Schrödinger equation is not real and is only representative of the averaged behaviours of the particle.

In this context, studying macroscopic systems exhibiting analog behaviours to quantum systems is attractive. First because they are convenient for quantum physics vulgarization in a pedagogical point a view. Second because they could bring advances in the understanding of quantum physics.

A. Chaotic cavities : the stadium case

The stadium billiard is a 2D geometry which consists in two semi-circles separated along their axis of orthogonal symmetry, as shown in Fig. 1. This seemingly simple geometry was one of the first shown to be non-integrable (a.k.a. chaotic) despite the absence of concave borders by Bunimovich [5], and is thus also called Bunimovich stadium. The difference in behaviour between classical and quantum particles has raised scientific attention in recent decades for such geometry [6–9]. A classical particle moving in straight lines and bouncing elastically on the borders of the stadium generally[1] leads to unpredictable motion despite the knowledge of the deterministic laws guiding its motion. The classical particle tends to visit the entire phase space [11] no matter its initial conditions. This ends up in a uniform probability to observe the classical particle inside the geometry. For a quantum particle (electron in most cases) trapped in a stadium cavity, the stationary eigenmodes of the wavefunction $\Psi(\mathbf{r})$ give a non uniform probability of presence $|\Psi(\mathbf{r})|^2$ where $\mathbf{r}$ is the position inside the geometry. Furthermore, they concentrate in the vicinity of the unstable periodic orbits of the classical particle. These phenomena are known as *scars* and have been observed in various quantum systems [12–14].

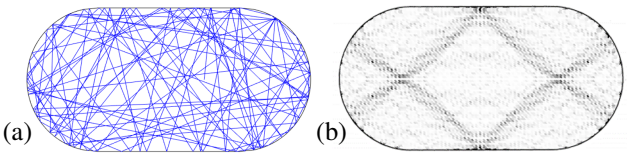

Fig. 1: (a) Simulated chaotic trajectory of a ball moving frictionlessly and bouncing elastically on the borders. (b) Simulated 2504th eigenmode for electrons confined in a stadium billiard.

B. Walking droplets

The first example of a macroscopic system exhibiting a wave-particle duality has been raised in 2006 by Couder et al. [15]. This consists in a silicone oil droplet bouncing on a vertically vibrated bath, generally sinusoidally. With an appropriate set of forcing parameters (i.e. frequency and amplitude of the vertical shaking), this droplet can spontaneously start "walking" on the liquid surface (i.e. moving laterally) and in this case exhibits behaviours thought to be exclusive to the microscopic quantum realm such as self-organising lattice structures [16], single particle diffraction [15], quantized orbits [17,18], tunneling effects [19], and wave-like statistics in confined geometries [20,21] among others. A droplet spontaneously walking on the vibrated liquid surface is called *walker* or *walking droplet*.
Given the contrasting behaviour between classical and quantum particles inside the stadium cavity, the central question of this paper is:

"*How does a walking droplet behave inside a stadium cavity?*".

Demonstrating that the walker faithfully reproduces the electronic behaviour, for example, would provide an easy table-top solution for exploring complex physical problems related to electron dynamics, correlated electron behaviour, including many-body effects that are otherwise extremely difficult to reproduce through simulations.

The issue for performing accurate experimental observations with walking droplets is that it requires the implementation of several features such as the control of the vertical shaking, the imaging of both the horizontal and vertical droplet dynamics, and the droplet

Identify applicable funding agency here. If none, delete this.

[1]There exists an infinite discrete set of unstable periodic orbits for the classical particle [10]

generation. Most of research laboratories developed their setup with costly equipment whose total cost reaches ten thousands euros in magnitude. This cost is generally unreachable for unfunded people.
In this paper, the creation of a complete low-cost and open-source setup for observing walking droplets from scratch is discussed and compared with analogous ones from research laboratories in Sec. II. All the data analysis routines and 3D conception drawings are available on a *Github* link, shortened as "the Github" in the next mentions.
The second part in Sec. III reports the first experimental observations conducted on walking droplets inside stadium cavities of various sizes. Motivated by the reasons given in Sec. III, the observations have been conducted on another setup from *ULiège*. In the next sections, the developed low-cost setup used for the observations will be written as *setup A* and *setup B*, respectively. It is observed that walking droplets generally converge towards stable trajectories similar to some scarring patterns observed with quantum particles.

II. Low-cost Experimental setup

This section aims at describing the low-cost self-developed setup and justifying the choices made in its conception. The different software programs as well as 3D drawings made with *Solidworks* are available in open-source on the Github. The first citations of components are clickable and link to their datasheet. A schematic of the experimental setup in shown in Fig. 2. The different aspects are discussed in their dedicated sections. A more detailed description can be found in [22].

A. Vertical shaking

A stadium-shaped bath made out of plexiglas has been fabricated and fixed on the membrane of a basic loudspeaker, playing the role of an electromagnetic shaker. The loudspeaker oscillates vertically with acceleration $\gamma(t) = \gamma_m \cos(\omega_0 t)$ where γ_m and $f_0 = \frac{\omega_0}{2\pi} = 80$ [Hz] are the prescribed maximum acceleration and frequency, respectively. The stadium of width $W = 38$ [mm] and length $L = 2W = 76$ [mm] has been designed such that $W \approx 8\lambda_F$, where λ_F is the Faraday wavelength, with the parameters in Table **??**. It is filled of silicone oil to a height $h_0 \in [6-11]$ [mm] (depending on the used stadium bath) such that a thin liquid film of depth $h_1 < 1.5$ [mm] overlays its border, serving as a wave damper. This choice instead of unsubmerged walls for delimiting the cavities prevents from the additional waves that would have been generated by the meniscus at the walls [23]. The used silicone oil comes from *Sigma-Aldrich*, with its physical properties given in Table **??**. The viscosity $\nu = 20$ [cSt] at $T = 25[°C]$ has been shown to be ideal for observing walkers with a frequency of forcing $f_0 = 80$ [Hz] [24].

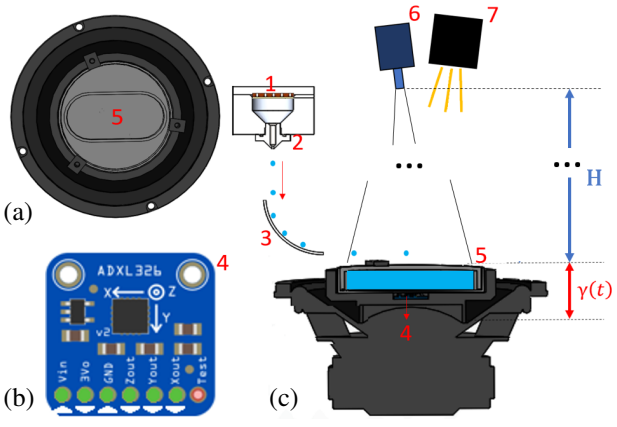

Fig. 2: (a) Top view of the experiment as seen by the camera. (b) Accelerometer used for the acceleration measurement. (c) Schematic of the experimental setup. 1 Piezoelectric- 2 Nozzle - 3 Launching pad - 4 Accelerometer - 5 Stadium - 6 Camera - 7 Lightning. The camera is placed at a height $H = 62$ [cm].

Following the dispersion relation of gravity-capillary waves [25], the liquid can be considered to have an infinite depth if the liquid height h_0 fulfils the condition :

$$\tanh(k_F h_0) \approx 1 \iff k_F h_0 > 4 \tag{1}$$

With $k_F = 1330$ [rad/m], (1) yields the condition $h_0 > 3$ [mm] which will always be satisfied in the following experiments.
The vertical forcing of the bath is ensured by a *NI Labview* program that communicates with a *NI myDAQ*. The electrical connections are shown in [22]. The *NI myDAQ* is able to actuate the loudspeaker through the use of a power amplifier, here a *Brüel & Kjaer type 2706*. The loudspeaker has carefully been positioned flat. External vibrations are partly reduced using anti-vibration foam and magnetic force. The acceleration measurement is performed using a 3-axis ± 16 [g] ADXL326 accelerometer, which is supplied with 5 [V] coming from a *Arduino Uno* and outputs a voltage in the range [0,3.3] [V] for each axis depending on the sensed acceleration in that direction. As there are only 2 AI with the myDAQ, the X and Y accelerations are measured with the AI of the Arduino Uno. Due to an unresolved enormous delay between the acceleration measurement and forcing (around 4 seconds), no initially intended PI controller was not used for an automatic convergence to the set point. The calibration of acceleration measurement is performed in [22].
The measured sinusoidal forcing is shown in Fig. 3. Some harmonics can be observed in Fig. 3(b), the related total harmonic distortion (THD) is :

$$THD = 100\frac{\sqrt{\sum_{h=2}^{H} v_h^2}}{\sqrt{\sum_{h=1}^{H} v_h^2}} = 1.7867[\%] \tag{2}$$

Where $h = 1$ is the fundamental component and $h > 1$ are the harmonics. $H = 8$ here. The transverse accelerations along X and Y axes are non-zero due to the lack of stabilization, they oscillate with the vertical forcing with an acceleration amplitude of 75 and 136 [mg], respectively. This issue discussed in [22] implies an effective Faraday threshold $\Gamma_{F,e}$ lower than the theoretical value Γ_F accompanied by an uncertainty on the actual memory parameter of the experiments.

B. Droplet generation

The diameter is an important parameter which influences the walking droplet dynamics [26,27]. Inspired from [28], a piezoelectric *Droplet on-demand generator* (DOD), shown in Fig. 2, has been designed to produce droplets of repeatable diameter ranging from 0.5 to 1.4 [mm]. Compared to [28], no pump for regulating the pressure is used. The pressure equilibrium at the nozzle outlet is ensured by aligning it with the top of the fluid reservoir. The piezoelectric buzzer is activated with square pulses generated by the switching of a bistable relay controlled by the Arduino Uno, and applied on the piezo. The amplitude V_s and width W_p are controllable by the Arduino Uno. The output droplet's diameter depends on the square pulse voltage amplitude V_s[V] and time width W_p[s] as well as on the nozzle outlet diameter n_D[mm]. The two first parameters are easy controllable on computer. Models of nozzles to be 3D printed are

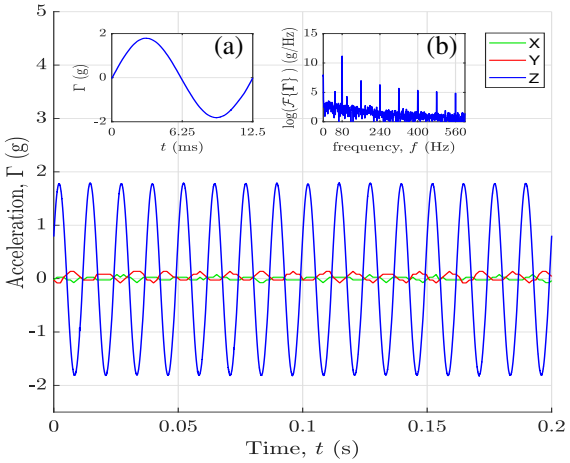

Fig. 3: Measured acceleration waveforms. The resulting root mean squared error wrt a perfect sinusoid is $RMSE = 52.75$ [mg]. The inset (a) is a zoom on one period. The inset (b) shows the spectrum (i.e. Fourier transform $\mathcal{F}\{\Gamma\}$) of the acceleration in logarithmic scale.

proposed on the Github, but require the DOD reservoir to be empty for changing it. The characterization results are shown in Fig. 4. From Fig. 4(a), it can be seen that averaging the diameter estimations over 10 selections or more leads to a confidence in the estimation lying within the $[-0.02, 0.02]$ [mm] interval. From Fig. 4(b), it can be seen that the difference between the generated droplets' diameters with the DOD remains lower than 0.1[mm] and allows for generating droplets of close diameters.

C. Imaging the walking droplets

A proper imaging of walking droplets is essential for an accurate measurement of both the droplets and the wave dynamics. The imaging techniques concerning the measurement of the wave and droplet's vertical dynamics are not covered as they are beyond the scope of this paper and matter less than the horizontal dynamics for the question of this paper. The developed low-cost setup has however been designed to handle such measurements, see discussion in [22]. From here, the analysis of droplet's horizontal dynamics will be named *Droplet tracking* or *Droplet detection*.
Images of the pilot-wave system are recorded with a familial *Panasonic DMC-FZ45* camera, with a framerate of 25 FPS and a resolution of 1080x720 pixels. As shown in Fig. 2, it is placed above the bath at a height $H = 62$[cm]. A desk lamp without occlusion is placed close to the camera and at the same height H to avoid heating the liquid whose properties vary with temperature. The images are post-processed with *Matlab* routines available on the Github. The criteria for an accurate droplet detection depend on the way the system is enlightened [22]. The one described here does not allow for a measurement of the wave dynamics but facilitates the tracking due to a higher contrast between the walking droplet and the background. For consistency with the observations given in Sec. III, the droplet tracking results depicted in Fig. 5 come from *setup B* and have been obtained using Algorithm 1 in Appendix A. The tracking results obtained on *setup A* remain similar to the ones from Fig. 5 up to the camera resolution level.
Note that the criterium for droplet detection in *setup A* is more sophisticated than choosing the darkest pixel for *setup B*. For each frame n, the droplet's center $\mathbf{c}$ is chosen as the position maximizing $|g_n[x, y]|$ with :

$$g_n[x,y] = (\mathbf{I}_n|_{\mathcal{R}_n} - \mathbf{I}_{n-1}|_{\mathcal{R}_n})[x,y] \cdot \left(\{\mathbf{I}_{n-1}|_{\mathcal{C}_n}, \mathcal{R}_n\} \circledast \mathbf{I}_n|_{\mathcal{R}_n}\right)[x,y] \quad (3)$$

Where a bold font denotes a vector or a matrix, $\mathbf{I}_n|_{\mathcal{R}}$ is the image at integer time frame n limited to the region of interest (ROI), $\mathcal{C}_n$ denotes the correlation zone set of coordinates at time frame n. $\{\mathbf{I}_{n-1}|_{\mathcal{C}_n}, \mathcal{R}_n\}$ stands for the interpolation to the size of $\mathcal{R}_n$ using fast Fourier transform (FFT). The correlation operation $\circledast$ is computed via FFT for reducing the computational cost.
In (3), the metric that is maximized is the combination (pointwise product) of an image difference (first line) and a correlation (second line).

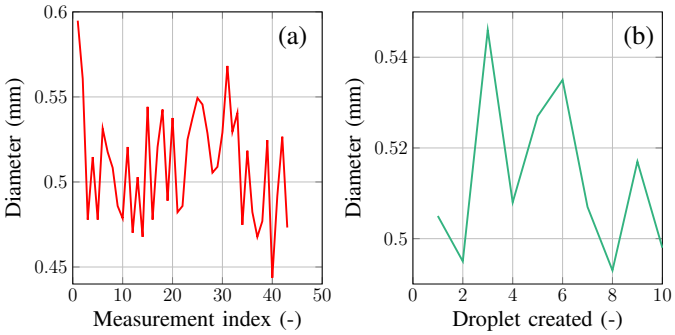

Fig. 4: (a) Estimations of the diameter of the same droplet on consecutive images. The measured mean is $D_m = 0.51$[mm] with standard deviation $\sigma_D = 0.032$[mm] over 43 measurements. (b) Estimations of different droplets' diameters generated with the same parameters (nozzle of diameter 1[mm], voltage $V_s = 50$[V] and pulse width Arduino command $W_p = 4700[\mu s]$) averaged over 20 different images.

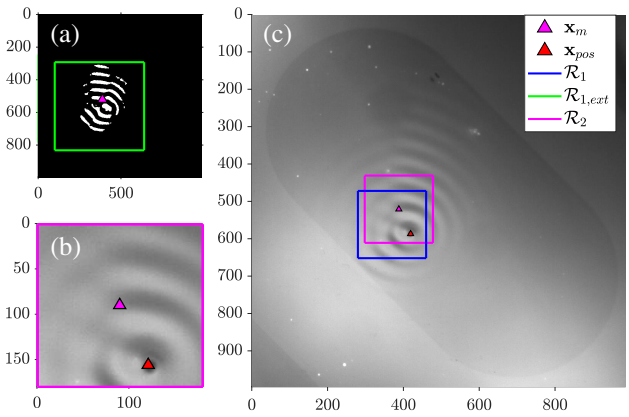

Fig. 5: Illustration of the droplet tracking using Algorithm 1. (a) Binary mask $\mathcal{M}$ with it associated region of interest (ROI) and center of mass. (b) Zoom on $\mathcal{R}_2$. (c) Full processed image with the search ROIs. One observes an accurate droplet detection.

D. Total cost

The desk lamp and the camera (a smartphone could be exploited) are likely already available for anyone thus no cost is associated. The cost contributions are depicted in Fig. 6. The *3D printing* part comprises the bath, reservoir and nozzles of the DOD. The most expansive component is the silicone oil only available in specialized industries.

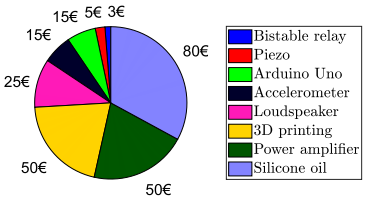

Fig. 6: Contributions to the total cost of 243€ for *setup A*. The variable delivery cost have not been taken into account.

III. Walking droplet experiment

The main drawbacks of the low-cost experimental setup (*setup A*) described in Sec. II are first that the loudspeaker shown in Fig. 2 is both too small and not powerful enough to ensure a quality sinusoidal shaking for larger baths, and second that no covering plate was designed to avoid any interaction between the walking droplet system and the external environment. In this context, the experimental results that will be shown in the section have been conducted with a similar more expansive setup (*setup B*) from *ULiege* (Belgium). The differences between setups A and B are reported in Table I.

The experimental setup, depicted in Fig. 7, comprises a circular bath of diameter 24 [cm]. Two baths with various stadium sizes (Fig. 7.(c-d)) have been used in the experiments, each composed of two different depths regions. The experimental zones, i.e. the stadium cavities (in white) are filled with $h_0 \approx 4.2$ [mm] of silicone oil, also satisfying (1). The stadiums in Fig. 7.(d) have been placed far enough (min 22 [mm]) to avoid any interaction [29]. The bath is placed on top of an electromagnetic shaker (V400LT, Data Physics). The shaker motion is accurately controlled via an accelerometer tightly fixed on the reservoir, a computer interface and a feedback loop, as detailed in [30]. The baths designs are available on the Github[2].

The five different stadium zones will be written Ω_i with $i = 1, \dots, 6$ ranging from largest to smallest. Their dimensions have been chosen wrt (with respect to) the Faraday wavelength $\lambda_F \approx 4.75$ [mm] and are shown in Table II.

The shaker is illuminated with 3 home-made high-power LEDs to obtain a uniform illumination of the bath. Thanks to a semi-refringent mirror placed at 45° above the shaker, optical paths of both illumination and recording are vertical near the bath surface. Thanks to a macro lens Zeiss Milvus 2/100M, the spatial resolution is brought down to 100 [µm] by pixel for the less resolved images. The scene is imaged by a Basler acA2040 camera with 2040×2048 pixels resolution. The camera is triggered by a DACQ (National Instruments) and a Labview interface to capture one image every 500 [ms] at the same phase wrt the droplet bounce. The captured images are post-processed with Matlab to compute the droplet's position following Algorithm 1 in Appendix A. For a fair comparison, the computed position coordinates are normalized in a reference stadium of dimensions 2×1 centered at the origin, as depicted in Fig. 8.

[2]go to Solidworks_Files/Liege

TABLE I: Main differences between setups A and B.

	Setup A	**Setup B**
Bath size	10 [cm]	24 [cm]
Lightning	All from top desk lamp	Semi-refringent high-power LEDs
Imaging	Basic camera non triggered	High-resolution camera triggered by $\gamma(t)$
-	/	Macro lens
Resolution	~ 60 [μm/p]	~ 120 [μm/p]
Shaking		PI controller
Anti-vibration	foam magnetic force	Springs included in the shaker
Insulation	/	Covering plate

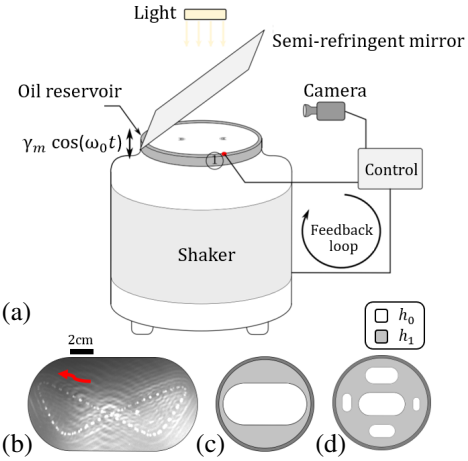

Fig. 7: (a) Experimental setup. (b) Top view of the experiment as seen by the camera. A superposition of multiple images is shown to highlight the droplet path. (c) (d) Design of the stadiums mounted on the shaker.

TABLE II: Stadium dimensions

Stadium	Ω_1	Ω_2	Ω_3	Ω_4	Ω_5	Ω_6
Radius [λ_F]	10	6	4	3	2	1.5

The following experimental results are accompanied by a triplet of parameter (Ω_i, D, Me) informing on the stadium used (see Table II), the droplet's diameter D (in [mm]) and the memory parameter (see Table **??**), respectively. The memory parameter [31] is defined as the ratio between the decay time constant τ and the Faraday period T_F :

$$Me = \frac{\tau}{T_F} = \frac{2\tau}{f_0} \tag{4}$$

It depends on the acceleration of the bath Γ induced by the vertical shaking as written in Table **??**. With the definition in (4), Me can be interpreted as the number of previous droplet bounces whose generated waves are still present on the liquid surface profile when the droplet bounces again.

Fig. 9 compares the trajectories of a walking droplet with five different initial positions. For each of these experiments, the memory is gradually increased. The color gradient informs that the droplet starts walking from its initial position, with a gradual speed increase taking around 20 [s], as shown in Fig. 9(c). A periodic drop of the

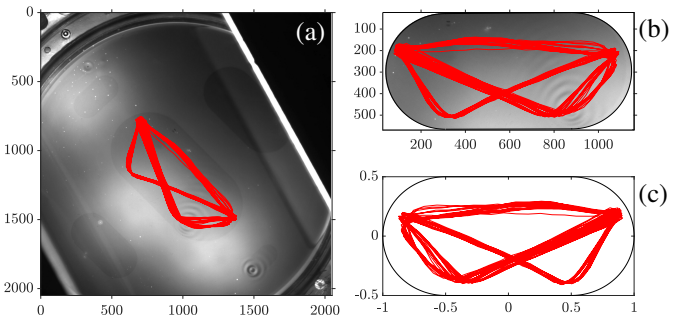

Fig. 8: (a) Trajectory in the original image. (b) Cutting out of the stadium and rotation up to horizontality. (c) Normalization of the trajectory.

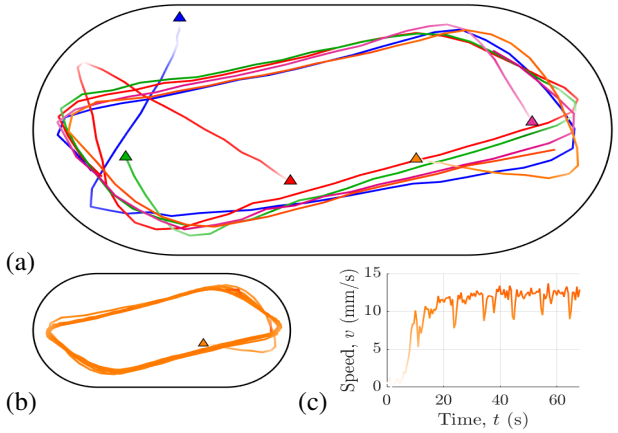

Fig. 9: $(\Omega_i, D, Me) = (\Omega_2, 0.77, 11.5)$ (a) Fast convergence of all initial conditions towards the same attractor. The triangles depict the initial position of the droplet. A color gradient whitens the line where the droplet's speed is low. (b) One entire trajectory. 23 cycles overlap. (c) Droplet's speed at early time.

speed related to the bounces on the edges of the stadium can also be seen in Fig. 9(c). It is observed the experiments all converge towards the same trajectory (a.k.a. *attractor*) of parallelogram-like shape after less than two bounces on the edges of the cavity. Only one loop inside the cavity is shown in Fig. 9(a) for the sake of clarity, but the stability of the attractor with time is highlighted in Fig. 9(b). The result shown seems to inform that the shape of the attractor is insensitive to the droplet's initial conditions. Some observations not shown here also seem to show that the diameter D does not influence the shape neither.

Fig. 10 highlights a drastic switch of stable trajectory due to a phase bounce change. The two observed attractors have a different shape than the one from Fig. 9, indicating the ratio between the Faraday wavelength λ_F (constant for these experiments) and the size of the cavity (see Table II) may be a influencing parameter. It also shows that the bounce phase, in other words the vertical dynamics of the walking droplet plays a crucial role in its interaction with the environment.

IV. Conclusion and perspectives

A. Discussion on the results

A low-cost open-source experimental setup for observing walking droplets was presented, with satisfying performances and a reduction factor of the total cost around 100 wrt funded research laboratories. The latter may be improved by implementing a PI controller for the vertical shaking and adding a covering plate for insulation.

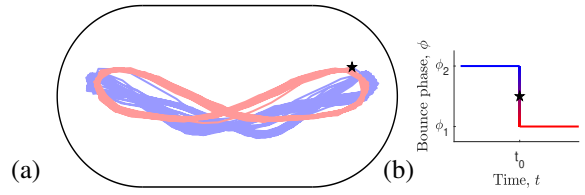

Fig. 10: $(\Omega_i, D, Me) = (\Omega_3, 0.67, 165)$ (a) Change of attractor due to a bounce phase change at reflection. The attractors in blue and in red contain 80 and 19 cycles inside the stadium, respectively. The time t_0 and position of the phase change are marked by a black star. (b) Sketch of the step in the bounce phase of the walking droplet.

The first observations of walking droplets inside stadium billiards were given. It was observed the wave-particle duality of walkers leads to stable trajectories similar to scarring patterns observed with electrons in the same geometry. The key parameters influencing this behaviour still need to be identified.

B. Perspectives for future research

This work opens many perspectives for further investigation in the comparison between the quantum world and the walking droplet pilot-wave system. First, the analysis could be deepened by comparing the 2D histogram of walking droplets inside the stadium cavities with the eigenmodes of the wavefunction $\Psi(\mathbf{r})$ inside a stadium billiard obtained by numerical simulations. Second, similar experiments could be performed in other chaotic geometries [5]. An analog to electron transport could also be studied by opening the stadium at one or multiple locations (*leads*), where the difference of potential between the leads would be translated in a difference of liquid depth, and an analog to conductance would be associated to the time spent by the droplet inside the billiard. This experiment would allow to look for an eventual periodic dependence of the transmission on the difference of potential, analog to recurrence observed in electron transmission vs electron energy [32]. One could also imagine to add the analog of magnetic field by making the whole system turn around the vertical axis, and observe if the walking droplet trajectories become curved, until presenting a behaviour similar to the Quantum Hall Effect [33] where, in the quantum case, the particles tend to follow the borders of the billiard.

Acknowledgment

The authors would like to thank Benoît Hackens, Nicolas Moreau, Boris-Brun Barrière and Corentin Félix from UCLouvain, as well as Loïc Tadrist, Tristan Gilet and Antonio Martinez from ULiège for their respective help contributions to this work.

Github link

https://github.com/reivilo3/Walking-droplet-in-stadium-cavity

Appendix A
Droplet tracking

The Algorithm 1 used for droplet position detection has been coded in *Matlab* and is available on the Github.

Algorithm 1: Droplet tracking

Input: d
Output: $\mathbf{x_{pos}} \in \mathbb{R}^{N\times 2}$

$\mathbf{I}_1 \leftarrow$ read() ; ▷ Initializations
$\mathbf{x}_{det}(1,:) \leftarrow$ user_click()
$\mathcal{R}_1 \leftarrow \{\mathbf{x} : |\mathbf{x} - \mathbf{x}_{pos}(1,:)| \leq d\}$
for $n = 2$ **to** N **do**
  $\mathbf{I}_n \leftarrow$ read()
  $\mathbf{I}_{\text{diff},n} \leftarrow \mathbf{I}_{n-1} - \mathbf{I}_n$; ▷ Image difference
  $\mathcal{M} \leftarrow \mathcal{H}(\mathbf{I}_{\text{diff},n}(\mathbf{x}))$, $\mathbf{x} \in \mathcal{R}_{1,\text{ext}}$; ▷ Hard thresholding
  $\mathcal{M} \leftarrow RSPN(\mathcal{M})$; ▷ Denoising
  $\mathbf{x_m} \leftarrow \mathrm{E}[\mathbf{x} \bullet \mathcal{M}]$, $\mathbf{x} \in \mathcal{R}_{1,\text{ext}}$; ▷ Center of mass
  $\mathcal{R}_2 \leftarrow \{\mathbf{x} : |\mathbf{x} - \mathbf{x_m}| \leq d\}$; ▷ ROI
  $\mathbf{x_{pos}}(n,:) \leftarrow \arg\min_{\mathbf{x}\in\mathcal{R}_2} \mathbf{I}_n(\mathbf{x})$; ▷ Darkest pixel
  $\mathcal{R}_1 \leftarrow \{\mathbf{x} : |\mathbf{x} - \mathbf{x}_{pos}(n,:)| \leq d\}$
end for
return $\mathbf{x_{det}}$

Where d is half the size of the ROIs $\mathcal{R}_1$ and $\mathcal{R}_2$, $R_{1,\text{ext}}$ is the extension of R_1 to a half size of $2d$, $\mathcal{M}$ is a binary mask of the image

TABLE III: **Properties and parameters.**

Name	Symbol	Value	[Unit]
SILICONE OIL			
Oil density	ρ	950	kg/m^3
Oil kinematic viscosity	ν	20	cSt (= mm^2/s)
Surface tension	σ	20.6	mN/m
DROPLET			
Droplet diameter	D	0.55–0.8	mm
SHAKING FEATURES			
Frequency of forcing	f_0	80	Hz
Non-dimensional acceleration peak[a]	Γ	3.8–4.5	–
Faraday wavelength	λ_F	4.75	mm
Non-dimensional Faraday threshold[a]	Γ_F	4.05–4.56	–
Distance to Faraday threshold	$\mathcal{M} = \frac{\Gamma_F}{\Gamma_F - \Gamma}$	8–500	–
Memory [31]	$Me = 0.765\,\mathcal{M}$	6–380	–

[a]Non dimensionalized by the acceleration constant $g = 9.81$ [m/s^2]

dimensions, $RSPN$ stands for *Remove Salt And Paper Noise* using mathematical morphology tools [34], $E[\mathbf{x} \bullet \mathcal{M}]$ is the expectation operator applied on the masked positions and $\mathcal{R}_2$ is the ROI for the search of the minimum. The choice of the darkest pixel is motivated by the imaging technique described in Sec. III and shown in Fig. 5. Note only two consecutive images are stored in memory in each iteration unlike the implicit notations used in line 5 for the sake of clarity.

REFERENCES

[1] H. Pierce Stapp, "The copenhagen interpretation," *American Journal of Physics 40(8):51-80, (2009)*.

[2] Wikipedia contributors, "Interpretations of quantum mechanics," https://en.wikipedia.org/wiki/Interpretations_of_quantum_mechanics, (2020), [Online; accessed 27-May-2020].

[3] Y. Couder, E. Fort, S. Protière, A. Eddi, J. Moukhtar, E. Sultan, A. Boudaoud, C. H. Gautier, F. Moisy, and M. Rossi. *A macroscopic-scale wave-particle duality.*

[4] Wikipedia contributors, "De broglie-bohm theory," https://en.wikipedia.org/wiki/De_BroglieâĂŞBohm_theory, (2020), [Online; accessed 27-May-2020].

[5] L. A. Bunimovich, "*"On the Ergodic Properties of Nowhere Dispersing Billiards."*," *Commun. math. Phys. 65, pp. 295-312 (1979)* .

[6] E. J. Heller, "*"Bound-State Eigenfunctions of Classically Chaotic Hamiltonian Systems: Scars of Periodic Orbits."*," *Phys. Rev. Let., vol. 53, 1515 (1984)*.

[7] C. King, "*"Exploring Quantum, Classical and Semiclassical Chaos in the Stadium Billiard."*," *Quanta (2014); 3: 16–31*.

[8] R. Akis, D. K. Ferry, and J. P. Bird, "*"Wave Function Scarring Effects in Open Stadium Shaped Quantum Dots."*," *Phys. Rev. Let., vol. 79, 123 (1997)*.

[9] L. Huang, Y.-C. Lai, D. K. Ferry, S. M. Goodnick, and R. Akis, "*"Relativistic Quantum Scars."*," *Phys. Rev. Let., vol. 103, 054101 (2009)*.

[10] J. Lei and X. Li, "*"Some dynamical properties of the stadium billiard."*," *Physica D: Nonlinear Phenomena, Volume 189, Issues 1–2, 15, Pages 49-60, (2004)*.

[11] C. P. Dettmann, C. Orestis Georgiou P. Dettmann, and O. Georgiou, "*"Transmission and reflection in the stadium billiard: Time-dependent asymmetric transport."*," *Phys. Rev. Let. E83, 036212 (2011)*.

[12] S. Sridhar, "*"Experimental observation of scarred eigenfunctions of chaotic microwave cavities."*," *Phys. Rev. Let., vol.67, no.1, p785 (1991)*.

[13] T. Harayama, T. Fukushima, P. Davis, P. O. Vaccaro, T. Miyasaka, T. Nishimura, and T. Aida, "*"Lasing on scar modes in fully chaotic microcavities."*," *Phys. Rev. Let. E, vol.67, no.1, p. 015-207 (2003)*.

[14] P. Wilkinson, T. Fromhold, L. Eaves, F. Sheard, N. Miura, and T. Takamasu, "*"Observation of 'scarred' wavefunctions in a quantum well with chaotic electron dynamics."*," *Nature, vol. 380, no. 6575, pp. 608–610, (1996)*.

[15] E. Fort and Y. Couder, "*"Single-Particle Diffraction and Interference at a Macroscopic Scale."*," *Phys. Rev. Let. (2006), 97(15):154101*.

[16] A. Eddi, A. Decelle, E. Fort, and Y. Couder, "*"Archimedean lattices in the bound states of wave interacting particles."*," *EPL (Europhysics Letters), vol. 87, Number 5 (2009)*.

[17] A. U. Oza, M. Labousse, S. Perrard, and J. W. M. Bush, "*"Pilot-wave dynamics in a harmonic potential: Quantization and stability of circular orbits."*," *Phys. Rev. E 93, 033122 (2016)*.

[18] E. Fort, A. Eddi, A. Boudaoud, J. Moukhtar, and Y. Couder, "*"Path-memory induced quantization of classical orbits."*," *Proceedings of the National Academy of Sciences, vol. 107, no. 41, p. 17515–17520, (2010)*.

[19] A. Eddi, E. Fort, F. Moisy, and Y. Couder, "*"Unpredictable Tunneling of a Classical Wave-Particle Association."*," *Phys. Rev. Let. (2009), 102(24):240401*.

[20] D. M. Harris, J. Moukhtar, E. Fort, Y. Couder, and J. W. M. Bush, "*"Wavelike statistics from pilot-wave dynamics in a circular corral."*," *Phys. Rev. E, vol. 88, 011001(R) (2013)*.

[21] T. Cristea-Platon, P. J. Saenz, and J. W. M. Bush, "*Walking droplets in a circular corral : Quantisation and chaos.*" *Chaos 28, 096116 (2018)*.

[22] O. Leblanc, "Comparison between the walking droplet and the electron behaviour inside a chaotic stadium cavity, UCLouvain, Belgium (2020)," Master's thesis.

[23] J. Bechhoefer, V. Ego, S. Manneville, and B. Johnson, "An experimental study of the onset of parametrically pumped surface waves in viscous fluids," *Fluid. Mech, vol. 288, p. 325–350, (1995)*.

[24] S. Protiere, "*"Gouttes rebondissantes : une association onde-particule à échelle macroscopique."*," *Université Paris-Diderot - Paris VII, (2007)*.

[25] M. Phillips, "*"The Dynamics of the Upper Ocean."*," *Phys. Rev. Let., vol. 261, pp.37 (1977)*.

[26] O. Wind-Willassen, J. Molacek, D. M. Harris, and J. W. M. Bush, "*"Exotic states of bouncing and walking droplets."*," *Physics of Fluids 25, 082002 (2013)*.

[27] J. Molacek and J. W. M. Bush, "*"Drops walking on a vibrating bath : towards a hydrodynamic pilot-wave theory."*," *J. Fluid. Mech., vol. 727, pp. 612-647 (2013)*.

[28] D. M Harris, T. Liu, and J. WM Bush, "*"A low-cost, precise piezoelectric droplet-on-demand generator"*," *Experiments in Fluids 56(4), (2015)*.

[29] A. Eddi, E. Sultan, J. Moukhtar, E. Fort, M. Rossi, and Y. Couder, "*"Information stored in Faraday waves: the origin of a path memory."*," *J. Fluid Mech. (2011), vol. 674, pp. 433–463*.

[30] N. Sampara and T. Gilet, "Two-frequency forcing of droplet rebounds on a liquid bath," *Phys. Rev. E, vol. 94, no. 5, p. 53112–53120, (2016)*.

[31] L. Tadrist, J.-B. Shim, T. Gilet, and P. Schlaghec, "*"Faraday instability and subthreshold Faraday waves: surface waves emitted by walkers."*," *J. Fluid Mech. (2018), vol. 848, pp. 906-945*.

[32] D. Cabosart, A. Felten, N. Reckinger, A. Iordanescu, S. Toussaint, S. Faniel, and B. Hackens, "*"Recurrent Quantum Scars in a Mesoscopic Graphene Ring."*," *Nano Letters 17(3), (2017)*.

[33] Wikipedia contributors, "Quantum hall effect — Wikipedia, the free encyclopedia," https://en.wikipedia.org/wiki/Quantum_Hall_effect, (2020), [Online; accessed 11-June-2020].

[34] A. Ledda, "Mathematical morphology in image processing," p. 44, 01 2007.